Monthly Notices
of the
ROYAL ASTRONOMICAL SOCIETY

Mon. Not. R. Astron. Soc. **411,** 644–652 (2011) doi:10.1111/j.1365-2966.2010.17712.x

Challenging times: a re-analysis of NGC 5408 X-1

M. J. Middleton,★ T. P. Roberts, C. Done and F. E. Jackson

Department of Physics, University of Durham, South Road, Durham DH1 3LE

Accepted 2010 September 14. Received 2010 September 13; in original form 2010 April 26

ABSTRACT

The ultraluminous X-ray source, NGC 5408 X-1, is one of only three such objects to show a quasi-periodic oscillation (QPO) in its power spectrum. Previous analysis of this signal identified it with the well-studied type-C low-frequency QPO (LFQPO) seen in black hole binaries (BHBs), implying an intermediate mass black hole (IMBH). However, in BHBs this QPO has a centroid frequency which scales tightly with the position of the low-frequency break in the broad-band power spectrum. We use this relation to predict the frequency of the power spectral break in NGC 5408 X-1, and show that this is inconsistent with the break frequencies in both available, archival *XMM–Newton* observations. Thus the broad-band power spectral shape does not support this identification of the QPO.

The energy spectra also do not support an IMBH interpretation. They can be fit by a two-component model, best described by soft thermal emission at low energies, together with low-temperature, optically thick Comptonization producing a tail which dominates above 2 keV. The parameters of the tail are unlike those seen in any of the sub-Eddington BHB spectral states. The energy-dependent variability supports this deconvolution, as it is consistent with the soft thermal component below 2 keV diluting extreme variability of the high-energy tail. The only objects with similar spectra which have similar amounts of variability are the BHB, GRS 1915+105 and some extreme Narrow-Line Seyfert 1s. This suggests that NGC 5408 X-1 is in a similar super-Eddington state, placing a natural limit on the mass of $\leqslant 100\,M_{\odot}$. Its QPO could then be similar to the ultra-LFQPO seen occasionally in GRS 1915+105, consistent with a large stellar mass black hole. We suggest a model geometry which may explain the spectra and variability of highly super-Eddington sources.

Key words: accretion, accretion discs – black hole physics – X-rays: binaries – X-rays: individual: NGC 5408 X-1.

1 INTRODUCTION

Extragalactic X-ray sources with luminosities in excess of 10^{39} erg s^{-1} have now been widely detected in the nearby Universe (Fabbiano 1989; Miller & Colbert 2004; Roberts 2007). These are designated as ultraluminous X-ray sources (ULXs) if they are not coincident with the nucleus of their host Galaxy (i.e. an active galactic nucleus, AGN) nor correspond to a foreground or background object, e.g. a quasi-stellar object. They are too luminous to be powered by a sub-Eddington accretion flow in a stellar-mass black hole binary (BHB) unless substantial beaming of their emission is invoked (King et al. 2001), so either require super-Eddington mass accretion on to a stellar mass black hole, or sub-Eddington accretion on to an intermediate mass black hole (IMBH; see Colbert & Mushotzky 1999). Unambiguously distinguishing between these possibilities requires radial velocity measurements of the underlying binary motion to directly determine the mass (see e.g. Charles & Coe 2006). Until these become available, we can only use more indirect arguments to identify the nature of these objects, primarily by comparing the X- ray spectral and timing properties of ULXs with those of stellar-mass BHBs (see e.g. the review by Roberts 2007).

The X-ray spectra of ULXs can be fairly well described by a two-component (disc plus power-law) model, as commonly used for BHBs. Taking the disc temperatures at face value implies masses of order 10^2–$10^5\,M_{\odot}$ (Kaaret et al. 2003; Miller et al. 2003; Miller, Fabian & Miller 2004; Cropper et al. 2004; Dewangan et al. 2004; Roberts et al. 2005), favouring sub-Eddington accretion flows on to an IMBH (Colbert & Mushotzky 1999). However, the disc component generally does not dominate these spectra, and BHBs show that in these circumstances the derived disc radii vary dramatically, so cannot be used to estimate mass (Kubota & Done 2004). Kajava & Poutanen (2009) show that this 'cool disc' component varies

★E-mail: m.j.middleton@dur.ac.uk

as $L \propto T^{-3.5}$, implying that the radius of the thermally emitting material increases with increasing luminosity, in sharp contrast to the $L \propto T^4$ expected from a disc with constant inner radius (see also Feng & Kaaret 2009). The observed behaviour may instead be produced from a super-Eddington source powering a strong wind, where the photosphere of the wind expands with increasing luminosity (Shakura & Sunyaev 1973; King & Pounds 2003; Begelman, King & Pringle 2006; Poutanen et al. 2007).

While the 'disc' spectrum is ambiguous, the 'power law' is somewhat clearer in distinguishing between IMBH and stellar mass systems (or rather in distinguishing between sub- and super-Eddington accretion). Sources with the highest quality data show clear signs that the high-energy 'power-law' tail rolls over above 6 keV, so it is better fit by low-temperature thermal Comptonization (Stobbart, Roberts & Wilms 2006; Miyawaki et al. 2009). A rollover at such low temperatures is not seen in any of the sub-Eddington BHBs, so this suggests that ULXs are super-Eddington and in a new, *ultraluminous* state (Roberts 2007; Gladstone, Roberts & Done 2009, hereafter G09; Vierdayanti et al. 2010). Similarly, low-temperature thermal Comptonization is also required in the brightest narrow-line Seyfert 1s (NLS1s, e.g. RE J1034+396) and the brightest BHB in our own Galaxy, GRS 1915+105 (Zdziarski et al. 2001; Middleton et al. 2009; Ueda, Yamaoka & Remillard 2009). Super-Eddington accretion then implies a much smaller mass black hole in ULXs, of the order 10–100 $M_{\odot}$.

Another diagnostic of the nature of the accretion flow is its rapid variability as this is strongly correlated with spectral state. Sub-Eddington BHBs show power density spectra (PDS) which can be very roughly described by band-limited noise, with a low frequency break at ν_b from a slope of ν^0 to ν^{-1}, followed by a high frequency break, ν_h, to ν^{-2}. This broad-band noise is often accompanied by strong low frequency quasi-periodic oscillations (LFQPOs) which correlate with the low frequency break ($\nu_{\rm LFQPO} \approx 10\nu_b$; Wijnands & van der Klis 1999). The LFQPO increases in frequency, coherence and power as the source flux increases and the spectrum softens from a faint low-hard state through the hard-intermediate state up to the soft-intermediate state (van der Klis 2004; Belloni, Méndez & Homan 2005; Remillard & McClintock 2006). During this transition, the broad-band power spectrum narrows in νP_ν, with ν_b increasing while the power at high frequencies remains fairly constant (Done, Gierliński & Kubota 2007; Czerny et al. 2008).

Whilst the characteristic breaks are difficult to constrain in the low signal-to-noise ratio ULX data (see Heil, Vaughan & Roberts 2009), QPO features are much easier to measure. Three ULXs are known to demonstrate strong QPOs in their PDS, M82 X-1 (Strohmayer & Mushotzky 2003), NGC 5408 X-1 (Strohmayer et al. 2007, hereafter S07; Strohmayer & Mushotzky 2009, hereafter SM09) and, more recently, a second source in M82 (Feng, Rao & Kaaret 2010). Identifying these with the type-C LFQPO seen in sub-Eddington BHBs implies that these are all IMBHs (Casella et al. 2008; S07; SM09). However, it also implies that the power spectra should show a low frequency break, and that the energy spectra should be consistent with a low-hard or very high state as these are the states in which the LFQPO is seen. We re-analyse the data from NGC 5408 X-1, looking at both spectra and variability, and show that neither the energy spectra nor power spectra support the identification of the QPO with the standard LFQPO seen in sub-Eddington BHBs. Instead we show that the spectra, power spectra and variability as a function of energy are all better matched by a super-Eddington flow, implying a stellar mass compact object, in which case the QPO may be analogous to the milli-Hz QPOs seen in GRS 1915+105.

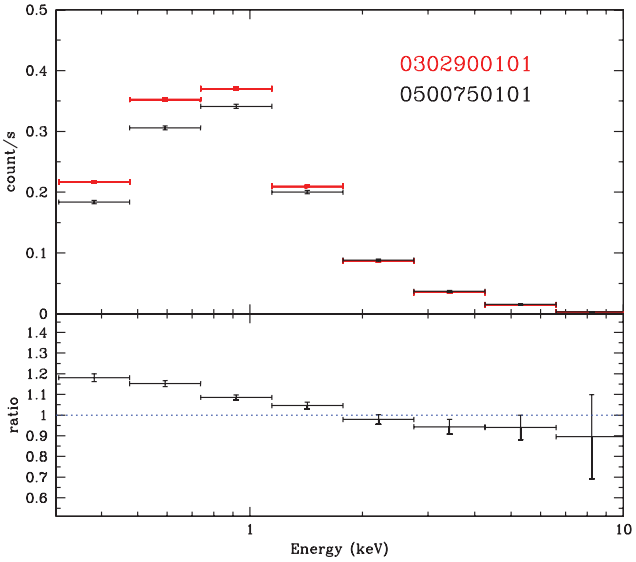

Figure 1. Mean count rate in each observation over the course of each respective GTI in the light curve. The ratio of the observations (Obs 1/Obs 2) demonstrates that count rate significantly drops between observations at soft energies below ∼1 keV but is consistent with staying the same at energies above this.

2 DATA EXTRACTION

The source was well exposed on two occasions for all three EPIC cameras on-board *XMM–Newton* (OBSIDs: 0302900101, hereafter Obs 1; 0500750101, hereafter Obs 2). These are separated by almost exactly 2 yr and have a duration of 132 and 116 ks, respectively.

We follow standard extraction procedure, reprocessing the raw data files in SAS v9.0 with up-to-date cross-calibration files. Taking extraction regions of 38 arcsec for both source and background (ensuring that the background region was within the central chip, far enough removed from the source to avoid point spread function wings and not coincident with other sources in the field of view), we extract light curves and spectra using XSELECT v5.10 and using patterns 0–4 and 0–12 for PN and MOS , respectively. The extracted light curves are found to be contaminated by background flares at the beginning and end of Obs 1, so excluding these gives a single good time interval (GTI) of ∼80 ks. However, for Obs 2, the background flares are more extensive, giving only ∼30 ks of continuous, clean data. This is in keeping with the data used for the recent rms-flux analysis of Heil & Vaughan (2010), but is markedly different to that of SM09 who used ∼70 ks from the light curve in Obs 2.

Fig. 1 shows the EPIC PN count rate as a function of energy for each observation, together with its ratio (Obs1/Obs2). Despite using different GTIs to S07 and SM09, we find a similar result, which is that there is a 20 per cent decrease at soft energies in Obs 2 compared to Obs 1, but that there is no significant change at hard energies.

3 ENERGY SPECTRA

For each observation we fit the EPIC PN and MOS spectra simultaneously in XSPEC 11.3.2, allowing the normalization of the model to float between the different instruments. The best-fitting values of these constants are consistent with each other to within 10 per cent in all the fits.

The spectrum of the first observation has been extensively studied by G09, where a break was found in the power-law component at

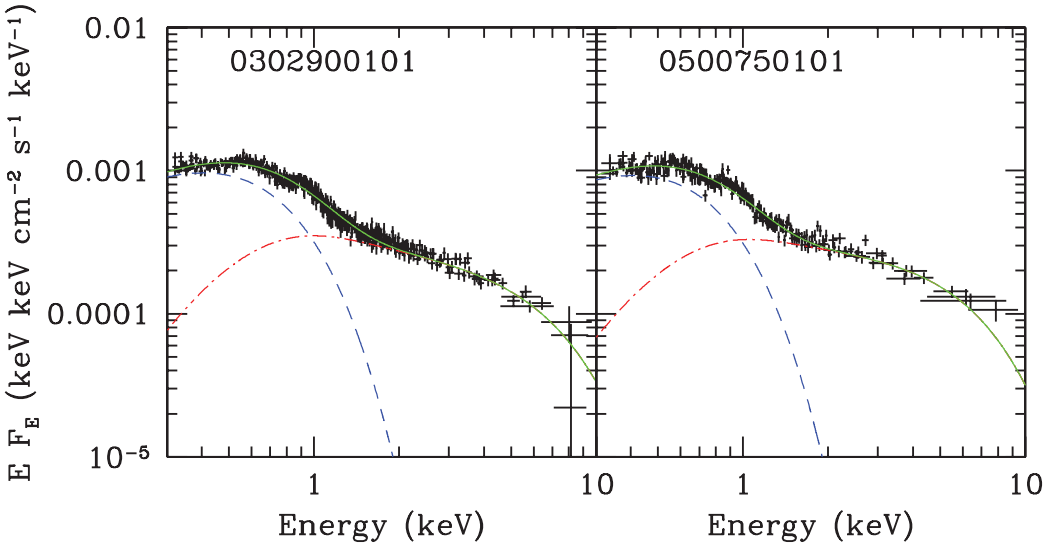

Figure 2. Energy spectra of combined EPIC MOS and PN observations of NGC 5408 X-1. Both spectra indicate a break around 2–3 keV or a deficit of photons in 1–2 keV band relative to the extension of the power law, fitted to the data above 4 keV. This can be interpreted as a signature of thermal Comptonization, thus the absorption-corrected convolution in green (solid line) is composed of a thermal disc component (DISKPN) in blue (dashed line), together with thermal Comptonization of the seed disc photons (COMPTT) in red (dot–dashed line).

Table 1. Table of best-fitting spectral parameters.

		DISKPN			COMPTT				
	$N_{\rm H}$	$T_{\rm max}$ (keV)	Norm ($\times10^{-3}$)	$F_{\rm d}$	$T_{\rm e}$ (keV)	τ	Norm ($\times10^{-4}$)	$F_{\rm c}$	χ^2
Obs 1	$9.6^{+0.8}_{-0.5}$	$0.17^{+0.00}_{-0.01}$	$2.9^{+0.1}_{-0.3}$	$1.6^{+0.7}_{-0.4}$	$1.6^{+0.4}_{-0.2}$	$6.3^{+0.9}_{-1.1}$	$5.8^{+7.7}_{-8.7}$	$1.2^{+1.1}_{-0.5}$	959 (829 d.o.f.)
Obs 2	$10.8^{+1.0}_{-1.3}$	$0.17^{+0.01}_{-0.00}$	$2.7^{+0.5}_{-0.9}$	$1.6^{+1.2}_{-0.6}$	$1.4^{+0.5}_{-0.3}$	$7.0^{+2.2}_{-1.5}$	$5.9^{+1.0}_{-1.2}$	$1.2^{+2.0}_{-0.6}$	637 (589 d.o.f.)

Note: best-fitting parameters for the model: TBABS*(DISKPN+COMPTT). $N_{\rm H}$ ($\times10^{20}$ cm^{-2}) is the neutral absorption column with the lower limit set at Galactic (5.73×10^{20} cm^{-2}), $T_{\rm max}$ is the peak disc temperature (with $R_{\rm in}$ set at $6R_{\rm g}$) which provides the seed photons for the electron plasma at temperature $T_{\rm e}$, τ is the optical depth of the same plasma and F is the 0.3–10 keV flux ($\times10^{-12}$ erg cm^{-2} s^{-1}) in the disc ($F_{\rm d}$) and Compton component ($F_{\rm c}$), respectively. All errors are 90 per cent confidence limits.

hard energies, consistent with other high quality ULX data. They showed that Obs 1 was in fact significantly better fitted by a disc plus low temperature Comptonization model than by a disc plus power-law model. Here, we revisit and improve that analysis, and apply a similar analysis to Obs 2 for the first time. We follow G09 and fit both observations with a DISKPN + COMPTT model, where DISKPN has $R_{\rm in}$ fixed at $6R_{\rm g}$. This is absorbed by a neutral column (TBABS) with lower limit set to that of Galactic absorption at 5.73×10^{20} cm^{-2} (SM09). The resulting best-fitting models are plotted with the de-absorbed data in Fig. 2, and the associated parameters are given in Table 1 together with their 90 per cent confidence limits.

The coronal component is cool ($T_{\rm e}\sim1.5$ keV) and optically thick ($\tau\sim7$) in both fits, providing a physical basis for the turnover evident at ∼4 keV in both spectra in Fig. 2. We assess the significance of this high energy break in the following, simple manner. We took the best-fitting model and fixed the temperature of the corona at (i) 100 keV, similar to the corona seen in the hard state (Ibragimov et al. 2005) and (ii) 20 keV, similar to that in the very high/steep power-law state (Kubota & Done 2004). We then re-fitted the model. In each case this led to a degradation in the quality of the fit, with $\Delta\chi^2>28$ for one additional degree of freedom (d.o.f.) for cases (i) and (ii) in Obs 1, and $\Delta\chi^2>14$ for Obs 2, compared to the free fit resulting in the cool corona. Statistically, this leads to >99.9 per cent confidence in all cases (according to the F-test) that the cool, optically thick solution provides a superior fit to the hotter corona cases. This argues strongly that the energy spectrum cannot be well described by classic sub-Eddington accretion states, as assumed by SM09.

Caballero-García & Fabian (2010) highlight that the spectrum of NGC 5408 X-1 contains line-like residuals at low energies (particularly below 1 keV; see their fig. 1). Introducing an optically thin plasma (MEKAL) component to each best-fitting model, to account for these features, significantly improved the fit ($\Delta\chi^2$ of 83 for 2 d.o.f. in Obs 1 and 50 for 2 d.o.f. in Obs 2, for a solar abundance MEKAL and a best-fitting temperature ∼0.8 keV). Previous work (SM09) has suggested that an extended X-ray component may be present, associated with the star formation regions close to NGC 5408 X-1 in its host Galaxy. One might naively assume that this plasma could originate in such a star-forming region. However, we note the large $L_{\rm X}$ from this plasma ($\sim2.6\times10^{38}$ erg s^{-1}) may be somewhat high for a small star-forming region in a small Galaxy; for context, the whole of M101 has a diffuse $L_{\rm X}$ of $\sim2\times10^{39}$ erg s^{-1} (Warwick et al. 2007). Furthermore, we find minimal evidence for extended emission in an analysis of the longest available *Chandra* data set (OBSID:4558). This suggests that the features are intrinsic to the source (as suggested by Caballero-García & Fabian 2010), which we will explore further in a future paper. In this paper, we are concerned only with the continua, and the parameters of this do not differ significantly from the fits reported in Table 1 after the addition of the MEKAL component.

4 TIMING ANALYSIS

4.1 Broad-band power spectra

We extract evenly sampled PDS for each observation using the XRONOS tool POWSPEC, from the background subtracted, co-added light curves of the EPIC PN and MOS detectors (using the same continuous GTI and extraction regions as used in the energy spectral analysis). Co-adding the data maximizes the total count rate and so maximizes the power spectral statistics. While the spectral response differs between PN and MOS detectors, the fractional variability at any specific energy should be perfectly correlated across both (although see Barnard et al. 2007 for possible, extraction-method-dependent problems).

As the observations are taken in full-frame mode, the maximum time resolution available across all three detectors is that for the MOS cameras of 2.6 s. However, in order to have sufficient statistics for a broad-band variability analysis, we use a time binning of 10 s. This binning gives an upper limit to the frequency range (0.05 Hz), just below the frequency at which the Poisson (white noise) errors become dominant.

S07 and SM09 show that the significance of the QPO (found at ∼0.01 and ∼0.02 Hz in Obs 1 and 2, respectively) is maximized over the energy bands 0.2–8 and 1–8 keV, respectively. We use the same energy bands to constrain the band noise power as this generally correlates with the QPO (McClintock & Remillard 2006). Our power spectra show the QPO at ∼0.01 and ∼0.02 Hz for Obs 1 and 2, respectively. The significance of these features has been confirmed in previous analyses (SM09; Heil et al. 2009) and so here we concentrate instead on the shape of the broad-band noise. If this QPO is the standard type-C LFQPO seen in BHBs, then the broad-band noise should break from ν^0 to ν^{-1} at a frequency which is a factor ∼10 lower than that of the QPO (Wijnands & van der Klis 1999). We can test for the presence and position of this break in our data and compare it to the expected and observed position of the QPO. In order to do this we use the entire length of each observation, calculating a PDS extending down to the lowest available frequencies (1/the length of the observation), so as to get the best possible constraints on a low frequency break. However, power spectral statistics mean that the uncertainty on the derived power is equal to the power itself leaving the continuum unconstrained. We get much better constraints from simulations, i.e. we create large numbers of simulated light curves with a model power spectrum which breaks from ν^0 to ν^{-1} at a frequency ν_b which we vary from 0.001 to 0.01 Hz. The simulated light curves have the same statistical properties as the original, including noise power (Middleton & Done 2010, see also Uttley & McHardy 2001), after which we obtain the average PDS of the simulated light curves, together with uncertainties given by the dispersion in the simulation values. These can then be compared to the real power spectra to get a χ^2 description of how well the simulations describe the data and hence constrain ν_b.

The upper and lower panels in Fig. 3 show reduced χ^2 against ν_b for the comparison between the simulations and the PDS for Obs 1 and 2. These are not smooth as power spectra are stochastic, but fitting the reduced χ^2 data with a quadratic allows us to determine the 90 per cent significance bounds ($\Delta\chi^2 = 2.7$).

This gives a lower limit on the break frequency of $>6.9 \times 10^{-3}$ Hz for Obs 1, while Obs 2 gives a detection at $4.0^{+1.2}_{-1.1} \times 10^{-3}$ Hz. Obs 1 is clearly inconsistent with the predicted break at 10^{-3} Hz for a type-C LFQPO at 0.01 Hz. The break in Obs 2 is closer to the type-C prediction of 2×10^{-3} Hz, but still outside the 90 per cent confidence interval allowed by the data. Thus the broad-band power spectral shape does not support the identification of the QPO with a type-C LFQPO.

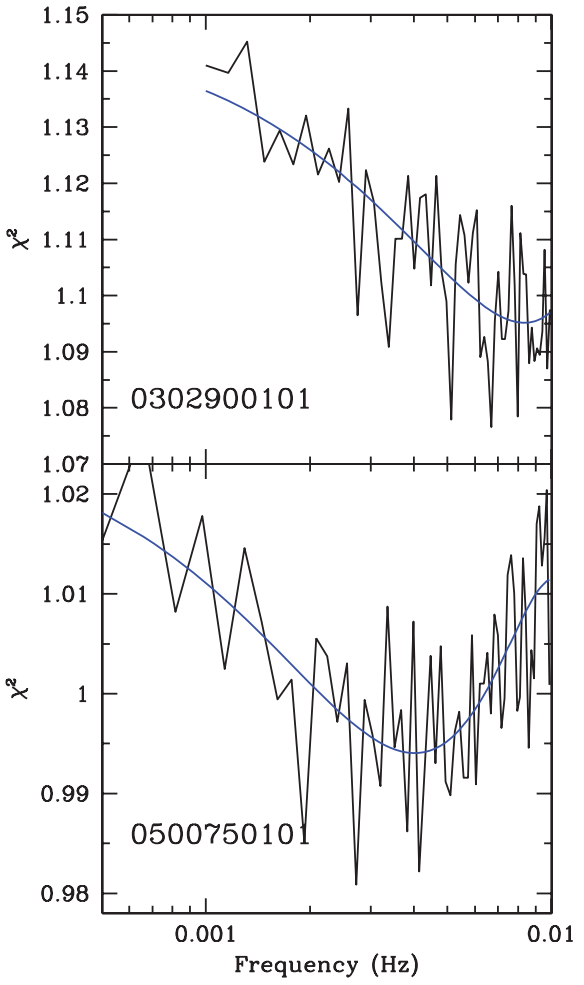

Figure 3. Panels showing the reduced χ^2 from simulating a large number of light curves with the same statistical properties as the original light curve. This allows us to test for the presence of a break by including the feature in the simulations across a suitable frequency range. In each case, the residual stochasticity is averaged by fitting a quadratic (Obs 1) or cubic (Obs 2) function (blue lines). In both cases, the well-constrained relationship between break frequency and QPO frequency (Wijnands & van der Klis 1999) predicts a type-C LFQPO at higher frequencies than those observed.

4.2 Energy-dependent variability

The energy spectrum compresses all variability information into a single average count rate, while a power spectrum compresses energy information. Here instead we combine the two approaches, looking at the energy dependence of the variability in order to disentangle different physical components in the spectrum.

Fig. 4 shows the average PDS of each observation, calculated from ∼80 (Obs 1) or 30 (Obs 2), 1000-s segments of the light curve. These are shown in soft (0.3–1 keV, magenta), hard (1–8 keV, green) and total (0.3–10 keV, black) bandpasses, where the normalization of the PDS is $(\sigma/I)^2$ (where σ^2 is the intrinsic, statistical error corrected, variance of the light curve and I is the mean count rate). Plainly there is more variability at hard energies than at soft energies, thus the total bandpass PDS lies between the two energy-resolved

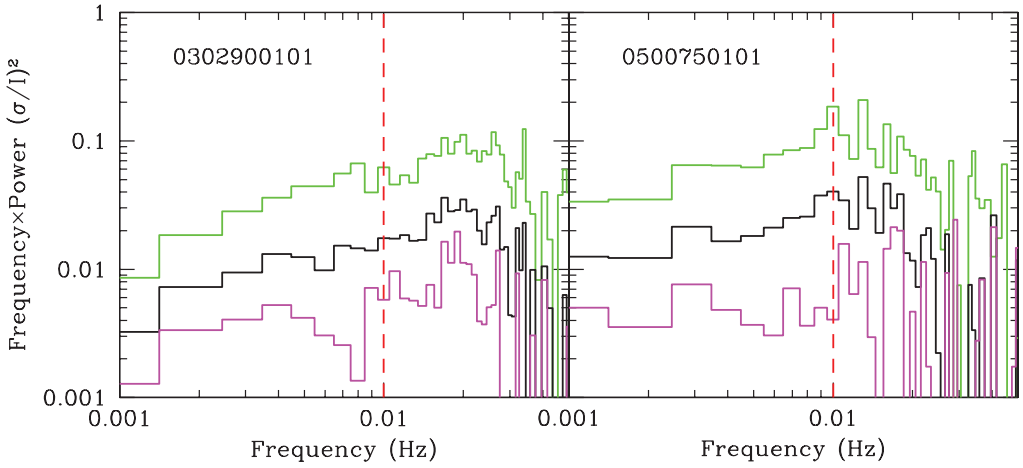

Figure 4. The average PDS for Obs 1 (left) and 2 (right) from 1000-s light curve segments in different energy bands. These have white noise subtracted and are geometrically rebinned by a factor of 1.02. This only has an effect at the highest frequencies, where it reduces some of the variance associated with white noise subtraction, but preserves the full (linear) resolution at lower frequencies. Green (upper histogram in both) corresponds to 1–8 keV, black (middle histogram in both) to 0.3–10 keV and magenta (lower histogram in both) to 0.3–1 keV, respectively. The vertical red line indicates the upper limit on the PDS sampled by the rms spectrum on 50-s binning (Fig. 5). Plainly there is more variability in the hard energy band than in the soft in both data sets.

PDS. There is also significantly more variability in the hard energy band in Obs 2 than Obs 1, with $\sigma/I = 0.426 \pm 0.008$ for Obs 1 increasing to 0.514 ± 0.013.

We get a more direct view of the energy dependence of the variability by calculating the rms variability spectrum, $\sigma/I(E)$ (see Edelson et al. 2002; Markowitz, Edelson & Vaughan 2003; Vaughan et al. 2003; Gierliński & Zdziarski 2005). To do this, we extract the total light curve over the length of the observation in each chosen energy bandpass (0.3–0.45, 0.45–0.7, 0.7–1.1, 1.1–1.8, 1.8–2.5, 2.5–10 keV). We first use 10-s binning, so we are in effect integrating the power spectrum in that energy band between frequencies of $1/T_{\rm obs}$ to the Nyquist frequency of 0.05 Hz. The results from this are shown by the black points in Fig. 5. In each observation, there is a very significant increase in rms from soft through to intermediate energies, peaking at an extraordinary 40 per cent in Obs 1 and ∼50 per cent in Obs 2! Following this peak, the fractional variability appears to flatten or perhaps even decrease at higher energies, though the lack of statistics at these energies means that this is not at all well constrained.

We can further resolve the variability by looking at long and short time-scales. We recalculate the rms using a binning of 50 s, to show only the power on long time-scales (red points). This shows a very similar pattern of variability to that derived from the total light curve, with much more variability at hard energies than at soft. The

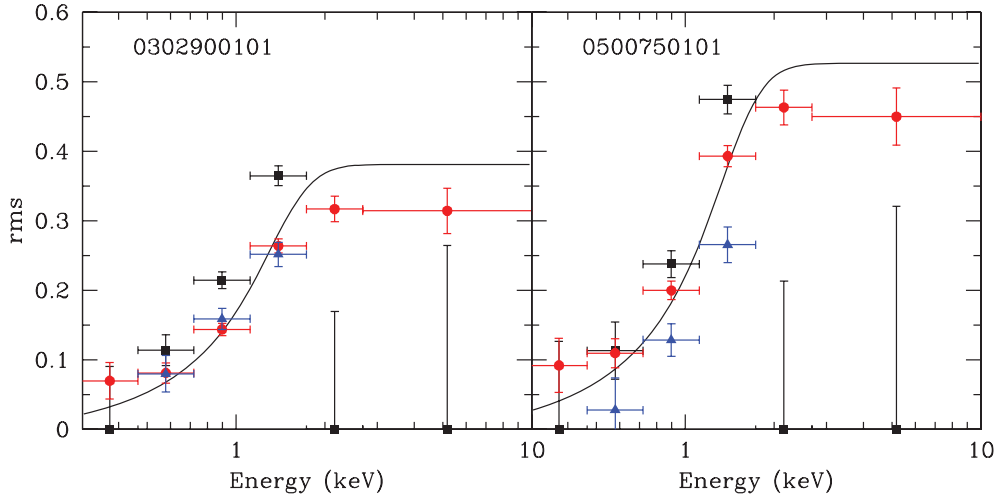

Figure 5. The rms spectra calculated from the light curves in each energy band. The black points (squares) correspond to the full frequency bandwidth i.e. from $1/T_{\rm obs}$ to the Nyquist frequency for 10-s binning. It is clear that the variability rises strongly with energy for both observations up to ∼1–2 keV. After this the signal-to-noise ratio is very poor so the variability may either level off or decrease with energy. There are only marginal differences in the pattern of variability with energy on different time-scales. The red points (circles) show the rms which results from calculating the rms from $1/T_{\rm obs}$ using 50-s binning of the light curve, so that it is more sensitive to the longer term variability (i.e. the PDS to the left of the vertical red line in Fig. 4), while the blue points (triangles) show the difference between these two, so that this gives the rms of the rapid variability, integrated over frequencies from $1/(2 \times 50)$ to $1/(2 \times 10)$ Hz. All these show that the amount of variability increases with energy up to 1–2 keV, consistent with the model where the variability at low energies is diluted by a constant soft component (black line).

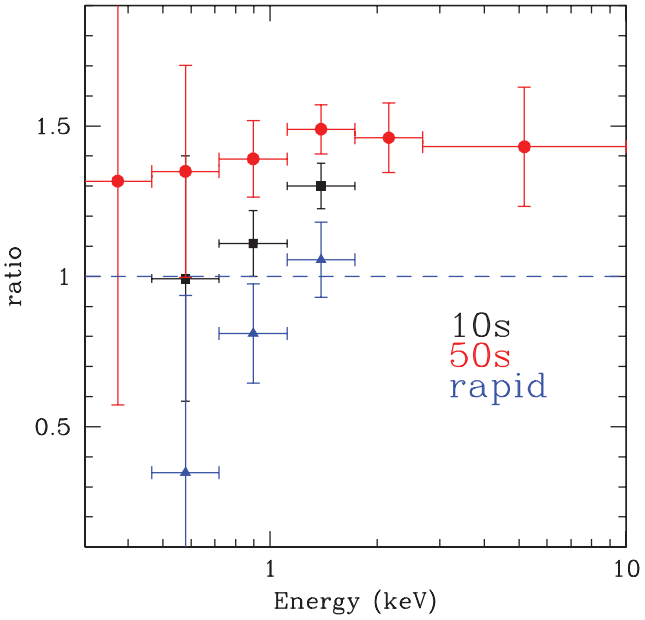

Figure 6. Ratio of the rms between Obs 2 and Obs 1, with fractional errors propagated through and respective colours (and shapes) corresponding to those in Fig. 5. Clearly the long time-scale variability (red circles) increases significantly ($>3\sigma$) between 1 and 3 keV from Obs 1 to Obs 2.

blue points show the energy dependence of the rapid variability, formed from the difference (in quadrature) between $\sigma/I(E)$ from the 10-s binning and that from the 50-s binning. Thus this effectively isolates variability between frequencies of 0.01–0.05 Hz, but again the pattern of variability with energy is very similar.

Both observations show a very similar pattern, but the rms variability at 1–2 keV is even larger for Obs 2 than Obs 1. The black points in Fig. 6 show the ratio of the total rms spectrum in Obs 2 compared to Obs 1, while the red and blue points show the ratio of rms for the long and short time-scale variability, respectively. Apart from on short time-scales, these show significantly more variability above 1 keV in Obs 2, as expected from the power spectral analysis (Fig. 4).

Thus, variability on all time-scales and in both observations shows a strong increase as a function of energy. This is consistent with a model in which there is a relatively stable component at soft energies diluting the variability as might be expected by a thermal disc (see Churazov, Gilfanov & Revnivtsev 2001) or optically thick photospheric component (G09; Zdziarski, Misra & Gierliński 2010). This can be modelled by changing the normalization of the hard energy spectral component by the percentage rms and taking the ratio of this to the best-fitting model. The result on 10-s binning is shown as the solid black line in Fig. 5, which closely resembles the shape of the rms.

We note that the shape of this rms is inconsistent with models in which the spectrum is dominated by a single component which changes only in normalization. This would give an rms which is constant with energy. This rules out the reflection dominated model of Caballero-García & Fabian (2010) unless the variability is strongly fine-tuned. The rms shape requires that the unseen illuminating power-law spectrum pivots around 0.3 keV (see the spectral and rms analysis of a reflection dominated model for RE J1034+396 in Middleton et al. 2009).

5 DISCUSSION

The spectral and rms analysis presented here both support a two-component model, where the soft component can be modelled by low-temperature thermal emission that is mostly constant on time-scales of up to a day, while the hard component, best modelled by a cool, optically thick corona, is steep and varies quite dramatically on time-scales down to at least a 100 s. Whilst this superficially resembles the properties of the 'steep power-law' state (McClintock & Remillard 2006) seen at fairly high luminosities, both the spectra and variability are inconsistent with such an interpretation. The low temperature of the thermal component means that if this were from an accretion disc then the black hole mass is of order $10^4\,M_\odot$. A similarly large mass is derived if the QPOs are identified with the BHB type-C LFQPO. However, the ULX luminosity of $\sim 10^{40}$ erg s^{-1} is then only $L/L_{\rm Edd} \sim 0.01$. BHBs have hard tails ($\Gamma \sim 1.5$–1.8) at such low mass accretion rates, rather than the soft tail[1] seen in NGC 5408 X-1. Similarly, the BHB power spectra at these low mass accretion rates show a low frequency break tightly correlated with the QPO frequency. These breaks are not present at the predicted frequency in NGC 5408 X-1.

Soft, variable tails are only seen in BHBs in the 'steep power-law' state, at $L/L_{\rm Edd} \sim 0.3$–1 (Remillard & McClintock 2006), giving a mass of 80–230 $M_\odot$ if NGC 5408 X-1 is in an analogous state. However, the large fractional variability of 0.3–0.4 is only seen above 10 keV in BHBs in this state, where the tail dominates over the constant disc component (see the energy-dependent rms spectra in Gierliński & Zdziarski 2005). Scaling this energy for the difference in mass from 80–230 $M_\odot$ to 10 $M_\odot$ gives a prediction that the tail should start to dominate above 4.5–6 keV, at significantly higher energies than seen in NGC 5408 X-1, where the variable tail dominates above 2 keV.

Thus, NGC 5408 X-1 does not look convincingly similar to any of the sub-Eddington BHB states. Instead, the large implied emission radius of the soft thermal component can also be incorporated into the super-Eddington flow models by identifying this not with the disc itself but with much more extended emission from the photosphere of a wind (Shakura & Sunyaev 1973; Begelman et al. 2006; Poutanen et al. 2007). Similarly, the extreme variability associated with the tail can be matched by occasional states of the pathologically variable BHB, GRS 1915+105, where it is probably associated with instabilities in a super-Eddington flow (Belloni et al. 1997). Fig. 7 (left-hand panel) shows the power spectrum of the tail in NGC 5408 X-1 (1–8 keV) compared to that of *RXTE* data from κ and μ variability states of GRS 1915+105 (centre panel, OBSIDs 20405-01-33-00; Belloni et al. 2000). These are calculated using standard 1 data (0.125-s resolution) which has no energy information, but the source spectrum in the *RXTE* bandpass means that the counts are concentrated in the 3–10 keV energy range. As well as showing similarly extreme amounts of broad-band noise, these also show small milli-Hertz QPO features at similarly low frequencies as seen in NGC 5408 X-1 (0.01 Hz for 33). These ultra-LFQPOs can dominate the power spectrum of GRS 1915+105 in other states where there is much less broad-band variability (OBSID: 10408-01-05-00 shown in magenta in the same panel), but this is unlike NGC 5408 X-1, where the QPOs are weak and the broad-band variability is strong. None the less, it is clear that stellar remnant black holes can produce ultra-LFQPOs as well as the standard type-C LFQPOs.

[1]The negative slope of the data at $E > 1.5$ keV in both panels of Fig. 2 demonstrates that $\Gamma > 2$, assuming a power-law fit, given the panels are plotted in Ef(E) space.

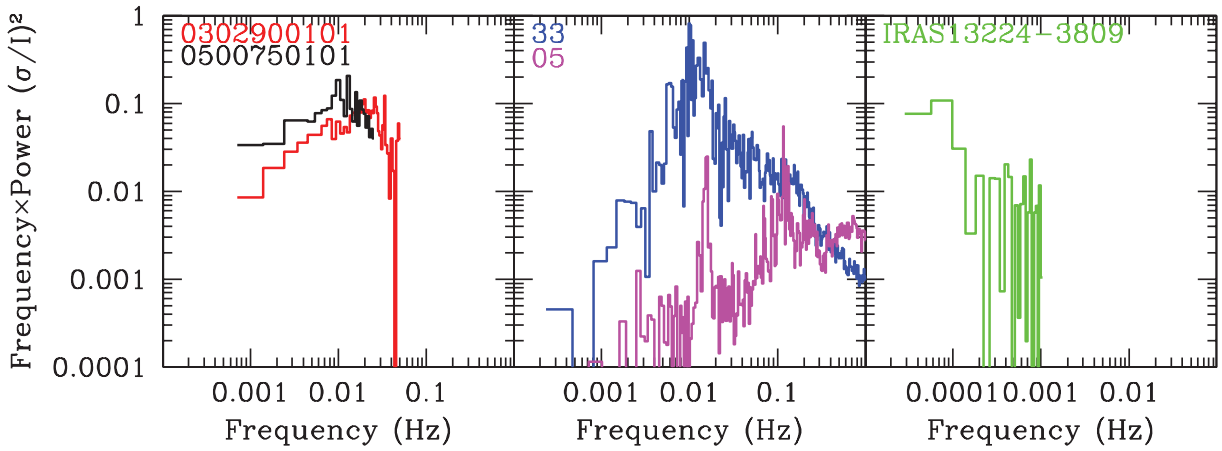

Figure 7. Left-hand panel: average (from 1000-s segments of the light curve) PDS of both observations of NGC 5408 X-1 in the 1–8 keV band. Centre panel: two PDS from *RXTE* observations of the BHB GRS 1915+105 in a highly luminous (probably super-Eddington) state (OBSIDs: 20405-01-33-00 and 10408-01-05-00, termed 33 and 05, in blue and magenta, respectively) created from the entire length of the observation. Right-hand panel: the *XMM–Newton* EPIC PN PDS of the NLS1 IRAS 13224−3809 created from the entire length of the observation. All PDS are very slightly geometrically rebinned (by a factor of 1.02) and have had their white noise subtracted. The amount of variability (i.e. the integrated power under the PDS) seen in the tail of NGC 5408 X-1 is unusually high and appears to only be matched by that seen in some super-Eddington sources.

However, while the variability properties of NGC 5408 X-1 and some states of GRS 1915+105 are very similar, the energy spectra are subtly different. The κ and μ state observations of GRS 1915+105 have spectra which can be well modelled by a disc plus low temperature, optically thick Comptonization (Zdziarski et al. 2001, 2005; Done, Wardziński & Gierliński 2004; Ueda et al. 2009, 2010), but *unlike* NGC 5408 X-1, the Comptonization component dominates the bolometric luminosity, rather than the thermal component (see Fig. 2, compared to Middleton & Done 2010).

Thus, even the most super-Eddington BHB is not really a good match to the spectrum of NGC 5408 X-1. The only known systems which show a similar combination of steep spectral tail and extreme variability are a small subset of NLS1s (Leighly 1999; O'Neill et al. 2005).[2] These are likely to be super-Eddington sources, but there are large uncertainties in deriving mass and mass accretion rate for these sources (Grupe & Mathur 2004; Marconi et al. 2008). Fig. 7 (right-hand panel) shows the power spectrum from *XMM–Newton* data (OBSID 0110890101) of the most extremely variable NLS1, IRAS 13224−3809 (Boller et al. 1997; Gallo et al. 2004; Ponti et al. 2010). Since any soft thermal component in the AGN should be at much lower energies, we use the full bandpass from 0.3 to 10 keV. Clearly the peak in $\nu P(\nu)$ reaches similar values, though the frequencies are very different.

Since NGC 5408 X-1 does not match with any of the sub-Eddington BHB states, nor to any of the multiple states of the mildly super-Eddington BHB GRS 1915+105, it seems most likely that it represents a strongly super-Eddington source. Such flows power a strong wind, where the wind photosphere gives the large radius, luminous, soft thermal component at low energies (Shakura & Sunyaev 1973; Begelman et al. 2006; Poutanen et al. 2007). This extended emission will be constant on short time-scales. We also see a much more variable tail, so the optically thick wind cannot cover all lines of sight to the inner disc. A reasonable geometry for this is an equatorial disc wind (Ohsuga 2007, 2009; Abolmasov, Karpov & Kotani 2009).

[2] However, we note that a second ULX with similar properties was reported while this paper was being reviewed (Rao, Feng & Kaaret 2010).

The low temperature, optically thick Compton emission could be produced by a corona over the inner disc, a more extreme version of the marginally optically thick corona seen in the steep power-law state (e.g. Done & Kubota 2006; G09). However, it could also be the spectrum of the inner disc itself as at such high mass accretion rate, the high disc temperature means that there is very little true continuum opacity (Beloborodov 1998, Done & Davis 2008). This means that the energy does not thermalize and cannot even be well approximated by a colour temperature corrected blackbody (see e.g. Watarai, Mizuno & Mineshige 2001). We favour this latter origin as the probably super-Eddington AGN RE J1034+396 shows clear evidence for a *separate*, variable corona, as well as a more constant low-temperature Comptonized component (the energy shift from the much larger black hole mass means that any wind photosphere emission is at too low an energy to be observed). This predicts there should also be an additional weak tail in the ULX, which is so far unobserved.

While the small size scale of the inner disc means that it could vary intrinsically, we note that other ULXs with similar spectra do not show similarly extreme variability (Heil et al. 2009, spectra from G09). Instead, a solution which can explain the range of variability behaviour in these wind-dominated ULXs could be if the extreme variability is extrinsic, from clumps in the wind. Numerical simulations show that this wind is turbulent (Ohsuga 2007; Ohsuga et al. 2009), giving strong variability of the Comptonization component from the inner disc on sightlines which intercept the major wind streamlines, but the soft thermal emission will remain mostly constant due to its much larger size scale.

We show a simple cartoon of this model in Fig. 8 (see also Leighly 2004). At extreme super-Eddington mass accretion rates, a large fraction of the accretion energy is ejected in the wind, making this energetically dominant (Poutanen et al. 2007). The photosphere of the wind (orange) is the source of soft thermal emission, while the inner disc (green) is the source of the low temperature, optically thick Comptonized emission. We propose that this has only low level intrinsic variability in strongly super-Eddington sources, perhaps because the disc structure is stabilized by advection (Abramowicz et al. 1988). Thus these sources have very low variability when viewed along a line of sight which does not intercept the wind, while

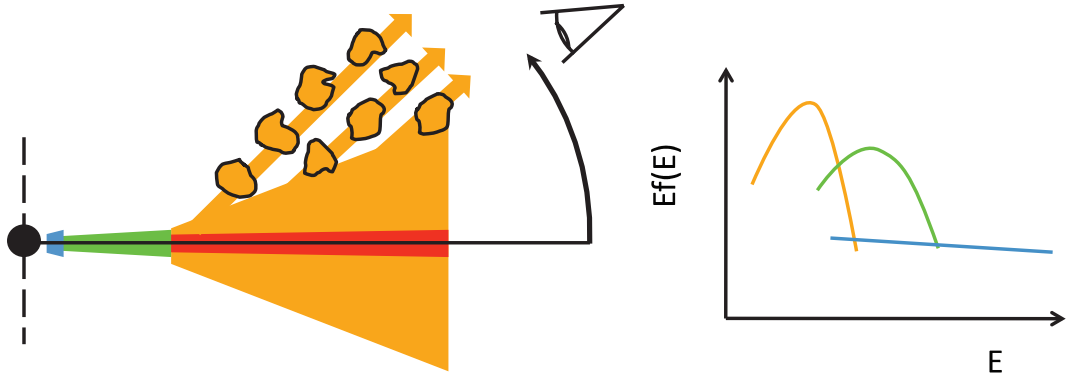

Figure 8. Cartoon of a physical model for high mass accretion rate sources. Here the quasi-thermal soft emission originates from a disc (red) distorted by a photosphere (orange) which is the base of the radiatively driven wind. The green region indicates optically thick Comptonization which is stable and blue indicates the most energetic region which is highly variable, appearing as optically thin Comptonization or a power law to higher energies. This is outside of the bandpass of ULXs as seen with *XMM–Newton* but is seen in GRS 1915+105 and certain NLS1s where the optically thick Comptonization can be seen to dilute the variability. This model suggests that, in the ULXs where variability is suppressed, we are viewing them directly along an unobscured line of sight to the central regions (hence they are close to face-on), but those which are highly variable such as NGC 5408 X-1, the obscuration of the optically thick, Comptonized emission region by a clumpy wind creates large-scale variability.

there is strong variability from obscuration of the Comptonized emission when viewed through the turbulent wind. The intrinsically variable, but rather weak corona (blue) gives rise to a weak high-energy tail, so far not observed in ULXs.

Scaling this model up to NLS1s could perhaps similarly explain the extreme variability from sources such as IRAS 13324−3809 and 1H0707−495 from absorption in strong winds (Gallo et al. 2004; see also Miller et al. 2010 for how this can also match the spectrum), the existence of which are supported by UV emission lines (Leighly 2004). The much lower variability seen from the low-temperature Comptonized component in RE J1034+396 is then associated with a more face-on viewing angle.

6 CONCLUSION

Where timing characteristics scale with mass, they can be used to determine the unknown mass of the black hole in ULX. However, the wide variety of properties seen in BHB means that this only works if the correct spectral state is identified for scaling. The key issue in ULXs is whether they are analogous to any of the classic, sub-Eddington, BHB states. If so, the large luminosities of these systems implies an IMBH. Instead, if ULXs are super-Eddington, then there are no well defined templates from BHB except for the unique source GRS 1915+105.

The suggested identification of the QPO in NGC 5408 X-1 is with the type-C LFQPO seen in BHBs. However, BHBs show a tight correlation between this QPO frequency and that of the low frequency break in the broad-band power spectrum (Wijnands & van der Klis 1999). We use extensive numerical simulations to constrain the position of this break in the two observations of NGC 5408 X-1, and find that they are inconsistent with the predicted frequencies from a type-C LFQPO.

The energy spectra of both observations of NGC 5408 X-1 are best described by a soft thermal component (disc or photosphere) together with a low temperature, optically thick, thermal Compton component, as proposed for other high-quality ULX spectra (G09). The rms spectra show that the variability increases strongly with energy, consistent with a constant soft component which dilutes a separate, strongly variable component at higher energies. The amount of variability in the high-energy component is extreme, and we speculate that this is extrinsic, from stochastic obscuration by the turbulent wind. The only objects with comparable variability and spectra are GRS 1915+105 and some extreme NLS1s, both of which are most probably super-Eddington accretors. This also suggests an alternative identification for the QPO in NGC 5408 X-1 as being more closely related to the ultra-LFQPO seen occasionally in GRS 1915+105. Both spectra and timing are then consistent with identifying NGC 5408 X-1 as a super-Eddington source. This places a natural upper limit on the central BH mass of $\sim 100\,M_{\odot}$, consistent with a BH formed from stellar collapse in a low-metallicity environment (e.g. Belczynski et al. 2010).

ACKNOWLEDGMENTS

We thank the referee, Juri Poutanen, for useful comments and insights. MJM thanks STFC for their support in the form of a post-doctoral position funded by a standard grant. This work is based on observations obtained with *XMM–Newton*, an ESA science mission with instruments and contributions directly funded by ESA member states and NASA.

REFERENCES

Abolmasov P., Karpov S., Kotani T., 2009, PASJ, 61, 213
Abramowicz M. A., Czerny B., Lasota J. P., Szuszkiewicz E., 1988, ApJ, 332, 646
Barnard R., Trudolyubov S., Kolb U. C., Haswell C. A., Osborne J. P., Priedhorsky W. C., 2007, A&A, 469, 875
Begelman M. C., King A. R., Pringle J. E., 2006, MNRAS, 370, 399
Belczynski K., Bulik T., Fryer C. L., Ruiter A., Valsecchi F., Vink J. S., Hurley J. R., 2010, ApJ, 714, 1217
Belloni T., Mendez M., King A. R., van der Klis M., van Paradijs J., 1997, ApJ, 479, L145
Belloni T., Klein-Wolt M., Méndez M., van der Klis M., van Paradijs J., 2000, A&A, 355, 271
Belloni T., Méndez M., Homan J., 2005, A&A, 437, 209
Beloborodov A. M., 1998, MNRAS, 297, 739
Boller T., Brandt W. N., Fabian A. C., Fink H. H., 1997, MNRAS, 289, 393
Caballero-García M. D., Fabian A. C., 2010, MNRAS, 402, 2559
Casella P., Ponti G., Patruno A., Belloni T., Miniutti G., Zampieri L., 2008, MNRAS, 387, 1707

Charles P. A., Coe M. J., 2006, in Lewin W. H. G., van der Klis M., eds, Compact Stellar X-ray Sources. Cambridge Univ. Press, Cambridge, p. 215
Churazov E., Gilfanov M., Revnivtsev M., 2001, MNRAS, 321, 759
Colbert E. J. M., Mushotzky R. F., 1999, ApJ, 519, 89
Cropper M., Soria R., Mushotzky R. F., Wu K., Markwardt C. B., Pakull M., 2004, MNRAS, 349, 39
Czerny B., Siemiginowska A., Janiuk A., Gupta A. C., 2008, MNRAS, 386, 1557
Dewangan G. C., Miyaji T., Griffiths R. E., Lehmann I., 2004, ApJ, 608, L57
Done C., Davis S. W., 2008, ApJ, 683, 389
Done C., Kubota A., 2006, MNRAS, 371, 1216
Done C., Wardziński G., Gierliński M., 2004, MNRAS, 349, 393
Done C., Gierliński M., Kubota A., 2007, A&AR, 15, 1
Edelson R., Turner T. J., Pounds K., Vaughan S., Markowitz A., Marshall H., Dobbie P., Warwick R., 2002, ApJ, 568, 610
Fabbiano G., 1989, ARA&A, 27, 87
Feng H., Kaaret P., 2009, ApJ, 696, 1712
Feng H., Rao F., Kaaret P., 2010, ApJ, 710, L137
Gallo L. C., Boller T., Tanaka Y., Fabian A. C., Brandt W. N., Welsh W. F., Anabuki N., Haba Y., 2004, MNRAS, 347, 269
Gierliński M., Zdziarski A. A., 2005, MNRAS, 363, 1349
Gladstone J. C., Roberts T. P., Done C., 2009, MNRAS, 397, 1836 (G09)
Grupe D., Mathur S., 2004, ApJ, 606, L41
Heil L. M., Vaughan S., 2010, MNRAS, 405, L86
Heil L. M., Vaughan S., Roberts T. P., 2009, MNRAS, 397, 1061
Ibragimov A., Poutanen J., Gilfanov M., Zdziarski A. A., Shrader C. R., 2005, MNRAS, 362, 1435
Kaaret P., Corbel S., Prestwich A. H., Zezas A., 2003, Sci, 299, 365
Kajava J. J. E., Poutanen J., 2009, MNRAS, 398, 1450
King A. R., Pounds K. A., 2003, MNRAS, 345, 657
King A. R., Davies M. B., Ward M. J., Fabbiano G., Elvis M., 2001, ApJ, 552, L109
Kubota A., Done C., 2004, MNRAS, 353, 980
Leighly K. M., 1999, ApJS, 125, 317
Leighly K. M., 2004, ApJ, 611, 125
McClintock & Remillard, 2006, in Lewin W. H. G., van der Klis M., eds, Compact Stellar X-ray Sources. Cambridge Univ. Press, Cambridge, p. 157
Marconi A., Axon D. J., Maiolino R., Nagao T., Pastorini G., Pietrini P., Robinson A., Torricelli G., 2008, ApJ, 678, 693
Markowitz A., Edelson R., Vaughan S., 2003, ApJ, 598, 935
Middleton M., Done C., 2010, MNRAS, 403, 9
Middleton M., Done C., Ward M., Gierliński M., Schurch N., 2009, MNRAS, 394, 250
Miller M. C., Colbert E. J. M., 2004, Int. J. Modern Phys. D, 13, 1
Miller J. M., Fabbiano G., Miller M. C., Fabian A. C., 2003, ApJ, 585, L37
Miller J. M., Fabian A. C., Miller M. C., 2004, ApJ, 607, 931
Miller L., Turner T. J., Reeves J. N., Braito V., 2010, MNRAS, 408, 1928
Miyawaki R., Makishima K., Yamada S., Gandhi P., Mizuno T., Kubota A., Tsuru T. G., Matsumoto H., 2009, PASJ, 61, 263
Ohsuga K., 2007, ApJ, 659, 205
Ohsuga K., Mineshige S., Mori M., Kato Y., 2009, PASJ, 61, L7
O'Neill P. M., Nandra K., Papadakis I. E., Turner T. J., 2005, MNRAS, 358, 1405
Ponti G. et al., 2010, MNRAS, 406, 2591
Poutanen J., Lipunova G., Fabrika S., Butkevich A. G., Abolmasov P., 2007, MNRAS, 377, 1187
Rao F., Feng H., Kaaret P., 2010, ApJ, 722, 620
Remillard R. A., McClintock J. E., 2006, ARA&A, 44, 49
Roberts T. P., 2007, Ap&SS, 311, 203
Roberts T. P., Warwick R. S., Ward M. J., Goad M. R., Jenkins L. P., 2005, MNRAS, 357, 1363
Shakura N. I., Sunyaev R. A., 1973, A&A, 24, 337
Stobbart A.-M., Roberts T. P., Wilms J., 2006, MNRAS, 368, 397
Strohmayer T. E., Mushotzky R. F., 2003, ApJ, 586, L61
Strohmayer T. E., Mushotzky R. F., 2009, ApJ, 703, 1386 (SM09)
Strohmayer T. E., Mushotzky R. F., Winter L., Soria R., Uttley P., Cropper M., 2007, ApJ, 660, 580 (S07)
Ueda Y., Yamaoka K., Remillard R., 2009, ApJ, 695, 888
Ueda Y. et al., 2010, ApJ, 713, 257
Uttley P., McHardy I. M., 2001, MNRAS, 323, L26
van der Klis M., 2004, preprint (astro-ph/0410551)
Vaughan S., Edelson R., Warwick R. S., Uttley P., 2003, MNRAS, 345, 1271
Vierdayanti K., Done C., Roberts T. P., Mineshige S., 2010, MNRAS, 403, 1206
Warwick R. S., Jenkins L. P., Read A. M., Roberts T. P., Owen R. A., 2007, MNRAS, 376, 1611
Watarai K.-y., Mizuno T., Mineshige S., 2001, ApJ, 549, L77
Wijnands R., van der Klis M., 1999, ApJ, 514, 939
Zdziarski A. A., Grove J. E., Poutanen J., Rao A. R., Vadawale S. V., 2001, ApJ, 554, L45
Zdziarski A. A., Gierliński M., Rao A. R., Vadawale S. V., Mikołajewska J., 2005, MNRAS, 360, 825
Zdziarski A. A., Misra R., Gierliński M., 2010, MNRAS, 402, 767

This paper has been typeset from a TEX/LATEX file prepared by the author.